The Integral Pulse Frequency Modulation Model With Time-Varying Threshold: Application to Heart Rate Variability Analysis During Exercise Stress Testing

Raquel Bailón*, Ghailen Laouini, César Grao, Michele Orini, Pablo Laguna, *Senior Member, IEEE*, and Olivier Meste, *Member, IEEE*

***Abstract*—In this paper, an approach for heart rate variability analysis during exercise stress testing is proposed based on the integral pulse frequency modulation (IPFM) model, where a time-varying threshold is included to account for the nonstationary mean heart rate. The proposed technique allows the estimation of the autonomic nervous system (ANS) modulating signal using the methods derived for the IPFM model with constant threshold plus a correction, which is shown to be needed to take into account the time-varying mean heart rate. On simulations, this technique allows the estimation of the ANS modulation on the heart from the beat occurrence time series with lower errors than the IPFM model with constant threshold (1.1% ± 1.3% versus 15.0% ± 14.9%). On an exercise stress testing database, the ANS modulation estimated by the proposed technique is closer to physiology than that obtained from the IPFM model with constant threshold, which tends to overestimate the ANS modulation during the recovery and underestimate it during the initial rest.**

***Index Terms*—Autonomic nervous system (ANS) modulation, exercise stress testing, heart rate variability (HRV), integral pulse frequency modulation (IPFM) model, respiratory sinus arrhythmia, time-varying mean heart rate, time-varying threshold.**

I. Introduction

THE integral pulse frequency modulation (IPFM) model has been proposed for studying the properties of biomedical signals, such as nerve spike trains [1], heart rate variability (HRV) [2], and for modeling the information coding and signal transmission through nervous fibers [3]. In the IPFM model, a spike is generated when the integral of a modulating signal reaches a threshold. Each time the threshold is reached, a spike is generated and the integral is reseted.

Several works have used the IPFM model to explain the regulation of the heart rate by the autonomic nervous system (ANS) [1], [4]–[11], where the ANS regulation is represented by the modulating signal and each spike generation represents a beat occurrence. Thus, the IPFM model can be used to estimate the ANS modulation on the sinoatrial (SA) node from the beat occurrence times, which is of interest in many physiological and pathological situations, in which the ANS activity may be altered, unbalanced, or damaged. Stress testing [12], tilt-table testing [13], and experiments of induced emotions [14] are some examples of these physiological situations, while myocardial infarction, diabetic neuropathy [15], and cardiac ischemia [16], [17] are examples of the pathological situations. In order to retrieve the ANS modulation on the SA node from the beat occurrence time series, different representations of HRV have been proposed, among which the heart timing signal has been demonstrated to provide an unbiased estimation of the ANS modulation, even in the presence of isolated ectopic beats [18], [19].

However, the IPFM model assumes a constant threshold, which in HRV analysis represents the mean heart period, not being appropriate in certain situations, in which the mean heart period is time varying, such as in exercise stress testing. In fact, the necessity of taking into account the time-varying heart period in the analysis of HRV during exercise stress testing was pointed out in [20] and [21], where a different approach, named the pulse frequency modulation model was applied to obtain the modulating signal. The analysis of the IPFM model with time-varying threshold has been previously addressed in [22], where the spectrum of the spike train output of the IPFM model is computed, in [23], where an IPFM model with periodically varied

Manuscript received July 5, 2010; revised October 12, 2010; accepted November 4, 2010. Date of publication December 6, 2010; date of current version February 18, 2011. This work was supported in part by the Ministerio de Ciencia e Innovación, Spain, under Projects TEC2010-21703-C03-02 and TRA2009-0127, in part by the Diputación General de Aragón, Spain, through Grupos Consolidados GTC ref:T30, in part by Instituto de Salud Carlos III, Spain, through CIBER CB06/01/0062, and in part by Caja de Ahorros de la Inmaculada de Aragón, Spain, through Programa Europa XXI. *Asterisk indicates corresponding author*.

*R. Bailón is with the Communications Technology Group (GTC), Aragón Institute of Engineering Research (I3A), University of Zaragoza, 50018 Zaragoza, Spain, and also with the Centro de Investigación Biomédica en Red en Bioingeniería, Biomateriales y Nanomedicina, 50018 Zaragoza, Spain (e-mail: rbailon@unizar.es).

G. Laouini is with the Laboratory of Informatics, Signals and Systems (I3S), University of Nice and CNRS, Sophia Antipolis 06903, France, and also with the Centro de Investigación Biomédica en Red en Bioingeniería, Biomateriales y Nanomedicina, 50018 Zaragoza, Spain (e-mail: laouini@i3s.unice.fr).

C. Grao is with the Communications Technology Group (GTC), Aragón Institute of Engineering Research (I3A), University of Zaragoza, María de Luna 1, 50018 Zaragoza, Spain.

M. Orini is with the University of Zaragoza, Zaragoza, 50018 Zaragoza, Spain, and also with Politecnico di Milano, 20133 Milano, Italy (e-mail: morini@unizar.es).

P. Laguna is with the Communications Technology Group (GTC), Aragón Institute of Engineering Research (I3A), University of Zaragoza, 50018 Zaragoza, Spain, and also with the Centro de Investigación Biomédica en Red en Bioingeniería, Biomateriales y Nanomedicina, 50018 Zaragoza, Spain (e-mail: laguna@unizar.es).

O. Meste is with the Laboratory of Informatics, Signals and Systems (I3S), University of Nice and CNRS, Sophia Antipolis 06903, France (e-mail: meste@i3s.unice.fr).

Digital Object Identifier 10.1109/TBME.2010.2095011

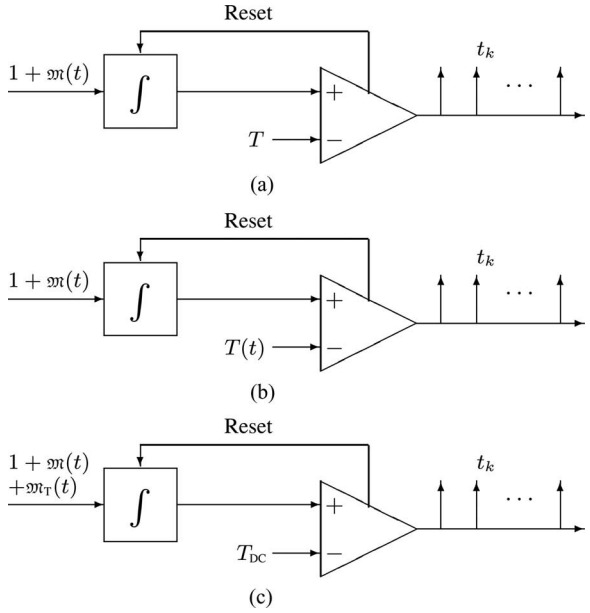

Fig. 1. Block diagram of the different IPFM models. (a) Classical IPFM model. (b) TVIPFM model. (c) Alternative TVIPFM model.

threshold is studied from the viewpoint of nonlinear dynamics, in [24], where a parametric approach is proposed to estimate the modulating signal as well as the time-varying threshold of the IPFM model, and in [25], where the effect of a time-varying threshold on the heart period is studied for a sinusoidal modulating signal.

In this paper, we propose an approach to the analysis of the time-varying threshold IPFM (TVIPFM) model applied to the analysis of HRV during exercise stress testing, which allows the estimation of the modulating signal using the methods derived for IPFM model with constant threshold plus a correction, which takes into account the time-varying threshold.

The paper is organized as follows. The IPFM model with constant and time-varying threshold are presented in Section II, where it is also described the simulation study designed to evaluate the performance of our approach, which simulates the beat occurrence time series during stress testing, as well as an exercise stress testing database, which is analyzed. Section III presents the results and Section IV a discussion of the proposed approach.

II. Methods and Materials

A. IPFM Model

In order to relate and derive the ANS influence on the beat occurrence time series t_k, which is the available information, we rely on the IPFM model. The IPFM model is based on the hypothesis that the ANS influence on the SA node can be represented by the modulating signal $\mathfrak{m}(t)$, and a beat trigger impulse is generated when the integral of $1+\mathfrak{m}(t)$ reaches a threshold T, which represents the mean heart period, resetting the integrator [5] [see Fig. 1(a)]. The modulating signal $\mathfrak{m}(t)$ is assumed to be causal, band-limited, and $\mathfrak{m}(t) < 1$.

Based on the IPFM model and assuming that the first beat occurs at time $t_0 = 0$, the beat occurrence time series can be generated as solution of

$$k = \int_0^{t_k} \frac{1+\mathfrak{m}(t)}{T} dt \tag{1}$$

where k and t_k represent the beat order and occurrence time of this kth beat [8], respectively. The term

$$d_{\mathrm{HR}}(t) = \frac{1+\mathfrak{m}(t)}{T} \tag{2}$$

represents the instantaneous heart rate in hertz, T is the mean RR interval (heart period) in seconds in the analyzed epoch, $1/T$ the mean heart rate, and $d_{\mathrm{HRV}}(t) = \mathfrak{m}(t)/T$ represents the HRV in hertz. Note that $d_{\mathrm{HRV}}(t)$ represents the time-varying part of the instantaneous heart rate $d_{\mathrm{HR}}(t)$.

The IPFM model can be generalized to continuous time rewriting (1) as follows [18]:

$$\kappa(t) = \int_0^{t} \frac{1+\mathfrak{m}(\tau)}{T} d\tau \tag{3}$$

where $\kappa(t)$ is the continuous beat-order function such that $\kappa(t_k) = k$.

Note that $d_{\mathrm{HR}}(t)$ can be obtained differentiating $\kappa(t)$ with respect to t, $d_{\mathrm{HR}}(t) = \kappa'(t)$, without any knowledge of T.

Then, the modulating signal $\mathfrak{m}(t)$ can be obtained by rewriting from (2) as follows:

$$\mathfrak{m}(t) = T \cdot d_{\mathrm{HR}}(t) - 1. \tag{4}$$

In practice, $\hat{\kappa}(t)$ is estimated by a spline interpolation of the pairs (t_k, k), then analytically derived to obtain $\hat{d}_{\mathrm{HR}}(t)$ [18], $\hat{T}$ is estimated as the mean heart period in the analyzed interval, and, finally

$$\hat{\mathfrak{m}}(t) = \hat{T} \cdot \hat{d}_{\mathrm{HR}}(t) - 1. \tag{5}$$

In situations, in which the mean heart period T is time varying, i.e., $T(t)$, such as during stress testing, the estimate $\hat{\mathfrak{m}}(t)$ in (5) also contains the variations of $T(t)$, which usually are of much lower frequency. For this reason, and to overpass this limitation, $\hat{\mathfrak{m}}(t)$ is usually high-pass filtered in order to remove the variations nonrelated to the modulating signal, assuming that these variations are of lower frequency and do not overlap with those related to $\mathfrak{m}(t)$. This estimate is denoted as $\hat{\mathfrak{m}}_0(t)$. As it will be shown in Section III, the amplitude of the variations of $\hat{\mathfrak{m}}_0(t)$ are still affected by the time-varying heart period $T(t)$, making $\hat{\mathfrak{m}}_0(t)$ a bias estimator.

B. IPFM Model With Time-Varying Threshold

In the TVIPFM model, the integral of $1+\mathfrak{m}(t)$ is compared to a time-varying threshold $T(t)$, representing the time-varying mean heart period, which can be decomposed as a constant component T_{DC} and a time-varying component $T_{\mathrm{AC}}(t)$, $T(t) = T_{\mathrm{DC}} + T_{\mathrm{AC}}(t)$ [24] [see Fig. 1(b)].

Assuming, as in Section II-A, that $\mathfrak{m}(t)$ is causal, band-limited, $\mathfrak{m}(t) < 1$, and that $T(t)$ is constant between two successive beats, the beat occurrence time series can be approximated

by

$$k \approx \int_0^{t_k} \frac{1+\mathfrak{m}(t)}{T(t)}dt \tag{6}$$

being the instantaneous heart rate

$$d_{\mathrm{HR}}(t) = \frac{1+\mathfrak{m}(t)}{T(t)}. \tag{7}$$

Assuming that the variations of the term $1/T(t)$ are slower than those of the term $\mathfrak{m}(t)/T(t)$, and that their spectral components do not overlap, a time-varying mean heart rate $d_{\mathrm{HRM}}(t)$ can be defined as follows:

$$d_{\mathrm{HRM}}(t) = \frac{1}{T(t)}. \tag{8}$$

Then, the HRV signal $d_{\mathrm{HRV}}(t)$ can be computed as follows:

$$d_{\mathrm{HRV}}(t) = d_{\mathrm{HR}}(t) - d_{\mathrm{HRM}}(t) = \frac{\mathfrak{m}(t)}{T(t)}. \tag{9}$$

From (9), it is evident that the modulating signal can be obtained by correcting the HRV signal $d_{\mathrm{HRV}}(t)$ by the time-varying mean heart rate $d_{\mathrm{HRM}}(t)$

$$\mathfrak{m}(t) = d_{\mathrm{HRV}}(t)T(t) = \frac{d_{\mathrm{HRV}}(t)}{d_{\mathrm{HRM}}(t)}. \tag{10}$$

Based on (7), different approaches can be considered for the estimation of the modulating signal $\mathfrak{m}(t)$.

1) Approach A: Equations (7), (8), and (9) can be seen from an alternative IPFM model with constant threshold, in which the effect on the output of the variations of the mean heart period $T_{\mathrm{AC}}(t)$ can be attributed to an extra modulating signal $\mathfrak{m}_{\mathrm{T}}(t)$, additional to $\mathfrak{m}(t)$, causal, band-limited, $\mathfrak{m}_{\mathrm{T}}(t) < 1$, and whose spectral components are lower than, and do not overlap with, those of $\mathfrak{m}(t)$. The block diagram of this alternative TVIPFM model can be seen in Fig. 1(c). If the variations of the time-varying threshold $T_{\mathrm{AC}}(t)$ are small compared to its mean value T_{DC}, the TVIPFM model of Fig. 1(b) and the alternative model of Fig. 1(c) can be shown to be approximately equivalent.

Let us start by rewriting (7)

$$\begin{aligned} d_{\mathrm{HR}}(t) &= \frac{1+\mathfrak{m}(t)}{T(t)} = \frac{1+\mathfrak{m}(t)}{T_{\mathrm{DC}}+T_{\mathrm{AC}}(t)} \\ &= \frac{1+\mathfrak{m}(t)}{T_{\mathrm{DC}}(1+T_{\mathrm{AC}}(t)/T_{\mathrm{DC}})} \\ &\approx \frac{1+\mathfrak{m}(t)}{T_{\mathrm{DC}}}\left(1-\frac{T_{\mathrm{AC}}(t)}{T_{\mathrm{DC}}}\right) \end{aligned} \tag{11}$$

such that, neglecting second-order terms, becomes

$$d_{\mathrm{HR}}(t) \approx \frac{1+\mathfrak{m}(t)-(T_{\mathrm{AC}}(t)/T_{\mathrm{DC}})}{T_{\mathrm{DC}}} \tag{12}$$

and, identifying terms in (2), $\mathfrak{m}_{\mathrm{T}}(t) = -T_{\mathrm{AC}}(t)/T_{\mathrm{DC}}$.

In this case, the instantaneous heart rate $d_{\mathrm{HR}}(t)$ can be obtained differentiating $\kappa(t)$ with respect to t, just as in Section II-A, as follows:

$$d_{\mathrm{HR}}(t) = \kappa'(t) \approx \frac{1+\mathfrak{m}(t)+\mathfrak{m}_{\mathrm{T}}(t)}{T_{\mathrm{DC}}}. \tag{13}$$

The time-varying mean heart rate $d_{\mathrm{HRM}}(t)$ is defined as follows:

$$d_{\mathrm{HRM}}(t) \approx \frac{1+\mathfrak{m}_{\mathrm{T}}(t)}{T_{\mathrm{DC}}} \tag{14}$$

and the HRV signal $d_{\mathrm{HRV}}(t)$ is computed as follows:

$$d_{\mathrm{HRV}}(t) \approx d_{\mathrm{HR}}(t) - d_{\mathrm{HRM}}(t) \approx \frac{\mathfrak{m}(t)}{T_{\mathrm{DC}}}. \tag{15}$$

Assuming

$$d_{\mathrm{HRM}}(t) \approx \frac{1+\mathfrak{m}_{\mathrm{T}}(t)}{T_{\mathrm{DC}}} \approx \frac{1}{T_{\mathrm{DC}}} \tag{16}$$

the expression in (10) is still valid. In order to estimate $\mathfrak{m}(t)$, the term $\hat{d}_{\mathrm{HR}}(t)$ is first estimated from (13), where $\hat{\kappa}(t)$ is obtained by spline interpolation of the pairs (t_k, k). Then, the term $\hat{d}_{\mathrm{HRM}}(t)$ is estimated by low-pass filtering $\hat{d}_{\mathrm{HR}}(t)$, and $\hat{d}_{\mathrm{HRV}}(t)$ is estimated from the middle term in (15). Finally, the estimate of $\mathfrak{m}(t)$, denoted as $\hat{\mathfrak{m}}_{\mathrm{A}}(t)$, is obtained from (10) as follows:

$$\hat{\mathfrak{m}}_{\mathrm{A}}(t) = \frac{\hat{d}_{\mathrm{HRV}}(t)}{\hat{d}_{\mathrm{HRM}}(t)}. \tag{17}$$

This approach allows the interpretation of the effect of a time-varying threshold on the IPFM model as due to an extra modulating signal $\mathfrak{m}_{\mathrm{T}}(t)$, different from $\mathfrak{m}(t)$, and to use the robust methods derived for the analysis of HRV based on the classical IPFM model with constant threshold [18], [19], which take into account the presence of ectopic beats.

2) Approach B: An alternative approach for the estimation of the modulating signal $\mathfrak{m}(t)$, which combines the results from the TVIPFM model with those of the IPFM model with constant threshold is the following.

Assuming that the quantity $d_{\mathrm{HR}}(t)$ is constant over two successive beat times ($t_{k-1} < t < t_k$), where no more information is available, the integration between two successive pulses may be computed by

$$\begin{aligned} 1 &= \int_{t_{k-1}}^{t_k} d_{\mathrm{HR}}(t)dt \approx d_{\mathrm{HR}}(t_{k-1})(t_k - t_{k-1}) \\ &\approx d_{\mathrm{HR}}(t_k)(t_k - t_{k-1}) \approx d_{\mathrm{HR}}\left(t_{k_c}\right)(t_k - t_{k-1}) \end{aligned} \tag{18}$$

where $t_{k_c} = (t_{k-1} + t_k)/2$ represents the in–between beat occurrence time.

Then, replacing $d_{\mathrm{HR}}\left(t_{k_c}\right)$ by its value in (7), we get

$$\mathfrak{m}\left(t_{k_c}\right) \approx \frac{T\left(t_{k_c}\right)}{(t_k - t_{k-1})} - 1 = \frac{T\left(t_{k_c}\right) - (t_k - t_{k-1})}{(t_k - t_{k-1})}. \tag{19}$$

The term $T(t)$ is estimated from $\hat{d}_{\mathrm{HRM}}(t)$, as in approach A, by $\hat{T}(t) = 1/\hat{d}_{\mathrm{HRM}}(t)$, and then evaluated at $t = t_{k_c}$. The term $\hat{T}\left(t_{k_c}\right)$ is substituted in (19) to obtain what is denoted as $\hat{\mathfrak{m}}_{\mathrm{B}}\left(t_{k_c}\right)$, and the continuous signal $\hat{\mathfrak{m}}_{\mathrm{B}}(t)$ is estimated by spline interpolation of the pairs $[t_{k_c}, \hat{\mathfrak{m}}_{\mathrm{B}}\left(t_{k_c}\right)]$. An alternative approach for the estimation of $\hat{T}(t_{k_c})$ is described in Appendix A.

3) Approach C: Yet another approach for the estimation of the modulating signal $\mathfrak{m}(t)$ based on the TVIPFM model can be

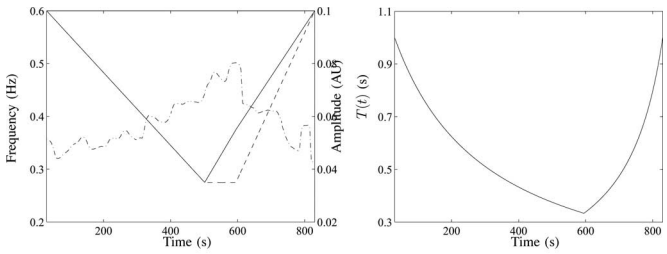

Fig. 2. Simulated signal: (a) $F_{\mathrm{HF}}(t)$ (dashed-dotted line), $A_{\mathrm{LF}}(t)$ (dashed line), and $A_{\mathrm{HF}}(t)$ (solid line); and (b) $T(t)$

considered [25] from (19)

$$\mathfrak{M}(t_{k_c}) \approx \frac{T(t_{k_c}) - (t_k - t_{k-1})}{T(t_{k_c})}. \tag{20}$$

The estimate in (20) is denoted as $\hat{\mathfrak{M}}_{\mathrm{C}}(t_{k_c})$; the continuous signal $\hat{\mathfrak{M}}_{\mathrm{C}}(t)$ can be estimated by spline interpolation of the pairs $[t_{k_c}, \hat{\mathfrak{M}}_{\mathrm{C}}(t_{k_c})]$.

C. Materials

1) Simulation Study: Due to the unavailability of a "true" reference-modulating signal representing the ANS regulation on the heart, a simulation study has been designed to evaluate the performance of the different approaches presented in this paper.

The ANS modulation during stress testing may be modeled by two sinusoids representing the low-frequency (LF) and high-frequency (HF) components, respectively. Thus, the analytic signal of the modulating signal $\mathfrak{m}(t)$ can be modeled as follows [12]:

$$a_{\mathfrak{M}}(t) = A_{\mathrm{LF}}(t)e^{j\Phi_{\mathrm{LF}}(t)} + A_{\mathrm{HF}}(t)e^{j\Phi_{\mathrm{HF}}(t)}. \tag{21}$$

The LF and HF components are defined by the amplitudes $A_{\mathrm{LF}}(t)$ and $A_{\mathrm{HF}}(t)$, and the instantaneous frequencies $F_{\mathrm{LF}}(t) = (1/2\pi)(d\Phi_{\mathrm{LF}}(t)/dt)$ and $F_{\mathrm{HF}}(t) = (1/2\pi)$ $(d\Phi_{\mathrm{HF}}(t)/dt)$, respectively. The very low frequency (VLF) component is not considered in this model since it cannot be estimated during stress testing. The $F_{\mathrm{LF}}(t)$ is assumed to be constant during the stress test and set to 0.1 Hz, while the $F_{\mathrm{HF}}(t)$ is set to be the respiratory frequency measured during a stress test recording using an airflow thermistor [26]. The frequency $F_{\mathrm{HF}}(t)$ and amplitudes $A_{\mathrm{LF}}(t)$ and $A_{\mathrm{HF}}(t)$ of the simulated signals are displayed in Fig. 2(a).

A time-varying mean heart period $T(t)$, displayed in Fig. 2(b), is simulated as the inverse of a time-varying mean heart rate, which increases linearly [27]–[29] from 60 bpm (1 Hz) at the beginning of the stress test to 180 bpm (3 Hz) at peak stress, and decreases linearly during recovery until the initial value of 60 bpm.

Given the modulating signal $\mathfrak{m}(t)$ and the time-varying threshold $T(t)$, the beat occurrence time series t_k is generated based on the TVIPFM model of Fig. 1(b). Then, the time series t_k are contaminated with additive white Gaussian noise (AWGN) in order to simulate the jitter in the QRS fiducial point of the estimated beat occurrence time series, i.e., $\hat{t}_k = t_k + v_k$, where

TABLE I
STUDY POPULATION CHARACTERISTICS

Group: # of subjects	Pedalling frequency (rpm)	$P_{\max}$ (W)	$\dot{V}_{O2peak}$ (ml·min^{-1}·kg^{-1})	Age (yr)
A: 2	70, 75	225± 10	37±2	33 ± 3
B: 9	(5)70, (3)75, 80	282±30	46±4	29±5
C: 3	(3)80	340±20	61±2	30±5
D: 9	(3)75, (3)85, (3)90	430±30	70±5	25±2

A: sedentary men; B: less than 10 hr training per week; C: more than 10 hr training per week, and D: high level athletes; $P_{\max}$: maximal power output; $\dot{V}_{O2peak}$: peak O_2 consumption.

v_k is a series of AWGN with variance σ^2. Different values of σ^2 (0.04×10^{-5}, 2.5×10^{-5}, and 10×10^{-5} s^2) have been considered representing different jitter in the QRS fiducial point (2, 5, and 10 ms, respectively).

A sampling frequency of 1000 Hz is used for the simulated $\mathfrak{m}(t)$ and $T(t)$.

2) Stress Testing Database: A database of stress testing recordings belonging to subjects with different training status is analyzed. All the subjects were nonsmokers and none was taking any medication. Physical activity, and alcohol and caffeine beverages consumption were prohibited 24 h before any exercise testing session. Following a 5-min resting period during which subjects stayed seated on the bicycle, all subjects performed a maximal graded exercise test with constant pedaling frequency, completing the exercise test without any clinical abnormality or discomfort. Initial workload and subsequent 2-min step workload increments were set to ensure a 12- to 15-min maximal exercise test. Subjects characteristics are shown in Table I, more information can be found in [30].

During the exercise test and the preceding 5 min (rest), a three-lead ECG was recorded and digitized online by a 12-bit analog-to-digital converter at a sampling rate of 1000 Hz on a personal computer.

Detection of the beat occurrence time series $\hat{t}_k$ is performed on one of the ECG leads, placed collinearly to the standard DII derivation directly on the chest in order to avoid limbs motion artifacts, after removing baseline with a high-pass finite impulse response filter.

D. Performance Measurements

In order to evaluate the different approaches, different performance measurements are considered. First, the estimated modulating signal $\hat{\mathfrak{m}}(n)$ is compared to the simulated modulating signal $\mathfrak{m}(n)$ (signals $\hat{\mathfrak{m}}(n)$ and $\mathfrak{m}(n)$ represent $\hat{\mathfrak{m}}(t)$ and $\mathfrak{m}(t)$, respectively, sampled at a sampling frequency of F_s (in Hz)). Then, clinical HRV parameters, namely the power of the LF and HF components, derived from $\hat{\mathfrak{m}}(n)$ ($\hat{P}_{\mathrm{LF}}(n)$ and $\hat{P}_{\mathrm{HF}}(n)$, respectively) are compared with those derived from $\mathfrak{m}(n)$ ($P_{\mathrm{LF}}(n)$ and $P_{\mathrm{HF}}(n)$, respectively). Parameters $P_{\mathrm{LF}}(n)$ and $P_{\mathrm{HF}}(n)$ are computed at each time instant n as follows:

$$P_{\mathrm{LF}}(n) = \frac{1}{2}\frac{1}{2K-1}\sum_{m=m_1}^{m_2} P_{\mathfrak{M}}(n,m)$$

$$P_{\mathrm{HF}}(n) = \frac{1}{2}\frac{1}{2K-1}\sum_{m=m_3}^{m_4} P_{\mathfrak{M}}(n,m) \tag{22}$$

TABLE II
PARAMETER VALUES

Parameter	$2M$	$2K-1$	γ	$2N-1$	m_1	m_2	m_3	m_4
Value (units)	1024 (samples)	1023 (samples)	$\frac{1}{64}$ (samples^{-1})	41 (samples)	$\lceil \frac{0.04}{F_s} M \rceil$ (samples)	$\lfloor \frac{0.15}{F_s} M \rfloor$ (samples)	$\lceil \frac{F_r(n)-0.07}{F_s} M \rfloor$ (samples)	$\lfloor \frac{F_r(n)+0.07}{F_s} M \rfloor$ (samples)

where $P_{\mathfrak{m}}(n,m)$ is the discrete smoothed pseudo Wigner–Ville distribution (SPWVD) of $\mathfrak{m}(n)$ defined as follows:

$$P_{\mathfrak{m}}(n,m) = 2\sum_{k=-K+1}^{K-1} |h(k)|^2 \times \left[\sum_{n'=-N+1}^{N-1} g(n') a_{\mathfrak{m}}(n+n'+k) a_{\mathfrak{m}}^*(n+n'-k)\right] \times e^{-\jmath 2\pi \frac{m}{M} k}; \quad m = -M+1,\ldots,M, \tag{23}$$

where n and m are the time and frequency indices, respectively, and $a_{\mathfrak{m}}(n)$ is the analytic signal of $\mathfrak{m}(n)$. The terms $g(n)$ and $|h(k)|^2$ represent the time and frequency smoothing windows, respectively, chosen to be

$$g(n) = \begin{cases} \dfrac{1}{2N-1}, & n = -N+1,\ldots,N-1 \\ 0, & \text{otherwise} \end{cases} \tag{24}$$

and

$$|h(k)|^2 = \begin{cases} e^{-\gamma|k|}, & k = -K+1,\ldots,K-1 \\ 0, & \text{otherwise.} \end{cases} \tag{25}$$

Parameter values used in the estimation of $P_{\mathrm{LF}}(n)$ and $P_{\mathrm{HF}}(n)$ are given in Table II, where the LF band is defined in its standard way from 0.04 to 0.15 Hz, while a time-varying HF band is defined centered on the respiratory frequency $F_r(n)$ (in Hz) with a bandwidth of 0.14 Hz [31]. Parameters $\hat{P}_{\mathrm{LF}}(n)$ and $\hat{P}_{\mathrm{HF}}(n)$ are computed from (22) and (23) substituting $\mathfrak{m}(n)$ with $\hat{\mathfrak{m}}(n)$.

For each value of σ^2, a total of $Q = 100$ realizations have been simulated. A relative error trend $e^q_{\theta\%}(n)$ is defined for each realization q and for each parameter $\theta(n)$, where $\theta(n) \in \{\mathfrak{m}(n), P_{\mathrm{LF}}(n), P_{\mathrm{HF}}(n)\}$

$$e^q_{\theta\%}(n) = \frac{\hat{\theta}^q(n) - \theta(n)}{\eta_\theta(n)} 100(\%). \tag{26}$$

The term $\hat{\theta}^q(n)$ represents the estimate of $\theta(n)$ in realization q, and the term $\eta_\theta(n) \in \{b_{\mathfrak{m}}(n), P_{\mathrm{LF}}(n), P_{\mathrm{HF}}(n)\}$, where $b_{\mathfrak{m}}(n)$ is the envelope of $\mathfrak{m}(n)$.

An averaged relative error trend $e_{\theta\%}(n)$ can be defined as follows:

$$e_{\theta\%}(n) = \frac{1}{Q}\sum_{q=1}^{Q} e^q_{\theta\%}(n). \tag{27}$$

For each realization q, the mean and SD of the error trends are computed and then averaged among the Q realizations, giving the performance measurements $\mu_{\theta\%}$ and $\sigma^2_{\theta\%}$

$$\mu_{\theta\%} = \frac{1}{Q}\sum_{q=1}^{Q}\frac{1}{N_q}\sum_{n=1}^{N_q} |e^q_{\theta\%}(n)|$$

$$\sigma^2_{\theta\%} = \frac{1}{Q}\sum_{q=1}^{Q}\frac{1}{N_q-1}\sum_{n=1}^{N_q}\left(|e^q_{\theta\%}(n)| - \frac{1}{N_q}\sum_{n=1}^{N_q}|e^q_{\theta\%}(n)|\right)^2 \tag{28}$$

where N_q is the number of samples of $\hat{\theta}^q(n)$.

III. RESULTS

A. Simulation Study

From the simulated $\hat{t}_k$ series, the modulating signal $\mathfrak{m}(n)$ is estimated using the approaches $\hat{\mathfrak{m}}_0(n), \hat{\mathfrak{m}}_{\mathrm{A}}(n), \hat{\mathfrak{m}}_{\mathrm{B}}(n)$, and $\hat{\mathfrak{m}}_{\mathrm{C}}(n)$, described in Sections II-A and B. A sampling frequency of $F_s = 4$ Hz and a fifth-order spline interpolation is used in all the approaches. The estimate $\hat{\mathfrak{m}}_0(n)$ is obtained by high-pass filtering $\hat{\mathfrak{m}}(n)$ with a cut-off frequency of 0.03 Hz, which is the same cut-off frequency used to obtain the time-varying mean heart rate $\hat{d}_{\mathrm{HRM}}(n)$. This cut-off frequency is below the lower limit of the LF band (0.04–0.15 Hz). The respiratory frequency $F_r(n)$ needed for the estimation of $P_{\mathrm{HF}}(n)$ is assumed to be equal to the instantaneous frequency of the HF component, and known.

Fig. 3 displays the SPWVD of the simulated modulating signal $\mathfrak{m}(n)$, as well as for $\hat{\mathfrak{m}}_0(n)$ and $\hat{\mathfrak{m}}_{\mathrm{A}}(n)$. It can be observed that $\hat{\mathfrak{m}}_{\mathrm{A}}(n)$ and $\mathfrak{m}(n)$ present similar characteristics, such as the progressive diminution of both the LF and HF amplitudes during the exercise, which is noticeable as lighter grays approximately from second 400 to 600. This effect cannot be appreciated in $\hat{\mathfrak{m}}_0(n)$, which presents even darker grays around the stress peak.

Table III displays the performance measurements obtained by the approaches proposed in this paper to estimate the modulating signal based on the TVIPFM model.

Regarding the parameters $\mu_{\mathfrak{m}\%} \pm \sigma_{\mathfrak{m}\%}$, it can be appreciated that all the three methods based on the TVIPFM model [$\hat{\mathfrak{m}}_{\mathrm{A}}(n), \hat{\mathfrak{m}}_{\mathrm{B}}(n)$, and $\hat{\mathfrak{m}}_{\mathrm{C}}(n)$] obtained notably lower values than the method based on the IPFM model with constant threshold [$\hat{\mathfrak{m}}_0(n)$], for all values of σ^2 considered, being the differences larger for lower values of σ^2. In the absence of noise, $\hat{\mathfrak{m}}_{\mathrm{A}}(n)$ obtained the lowest values, while the differences between $\hat{\mathfrak{m}}_{\mathrm{A}}(n), \hat{\mathfrak{m}}_{\mathrm{B}}(n)$, and $\hat{\mathfrak{m}}_{\mathrm{C}}(n)$ became insignificant when noise was added. Estimates $\hat{\mathfrak{m}}_{\mathrm{B}}(n)$ and $\hat{\mathfrak{m}}_{\mathrm{C}}(n)$ obtained slightly lower values than $\hat{\mathfrak{m}}_{\mathrm{A}}(n)$ for $\sigma = 5$ ms. Regarding the clinical HRV parameters ($\mu_{P_{\mathrm{LF}\%}} \pm \sigma_{P_{\mathrm{LF}\%}}$, and $\mu_{P_{\mathrm{HF}\%}} \pm \sigma_{P_{\mathrm{HF}\%}}$), approaches A, B, and C obtained much lower values than the

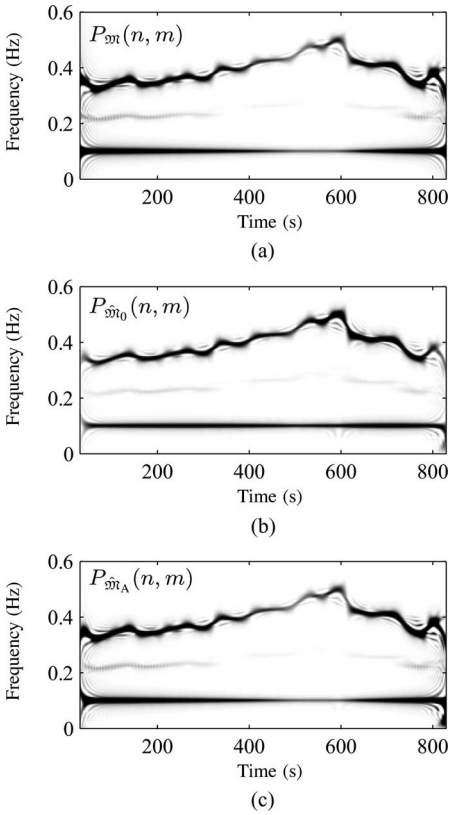

Fig. 3. SPWVD of (a) $\mathfrak{M}(n)$, (b) $\hat{\mathfrak{M}}_0(n)$, and (c) $\hat{\mathfrak{M}}_{\rm A}(n)$. In the gray scale, lighter grays stand for lower values and darker grays for higher values.

TABLE III
PERFORMANCE MEASUREMENTS $\mu_{\theta\%} \pm \sigma_{\theta\%}$ OBTAINED BY $\hat{\mathfrak{M}}_0(n), \hat{\mathfrak{M}}_{\rm A}(n), \hat{\mathfrak{M}}_{\rm B}(n)$, AND $\hat{\mathfrak{M}}_{\rm C}(n)$ FOR DIFFERENT VALUES OF σ

σ	$\mu_{\mathfrak{M}\%} \pm \sigma_{\mathfrak{M}\%}$ (%)			
(ms)	$\hat{\mathfrak{M}}_0(n)$	$\hat{\mathfrak{M}}_{\rm A}(n)$	$\hat{\mathfrak{M}}_{\rm B}(n)$	$\hat{\mathfrak{M}}_{\rm C}(n)$
0	15.0 ± 14.9	1.1 ± 1.3	3.6 ± 2.6	5.8 ± 4.9
2	18.4 ± 17.4	7.8 ± 7.8	7.4 ± 6.3	8.9 ± 7.1
5	28.1 ± 27.4	19.0 ± 18.9	16.1 ± 15.4	16.9 ± 15.4
σ	$\mu_{P_{\rm LF}\%} \pm \sigma_{P_{\rm LF}\%}$ (%)			
(ms)	$\hat{\mathfrak{M}}_0(n)$	$\hat{\mathfrak{M}}_{\rm A}(n)$	$\hat{\mathfrak{M}}_{\rm B}(n)$	$\hat{\mathfrak{M}}_{\rm C}(n)$
0	48.0± 31.0	0.9 ± 1.9	1.4 ± 1.9	1.2 ± 2.0
2	48.0 ± 31.1	1.5 ± 2.0	1.8 ± 2.1	1.7 ± 2.2
5	48.2 ± 32.9	3.9 ± 4.9	3.1 ± 2.7	3.1 ± 2.9
σ	$\mu_{P_{\rm HF}\%} \pm \sigma_{P_{\rm HF}\%}$ (%)			
(ms)	$\hat{\mathfrak{M}}_0(n)$	$\hat{\mathfrak{M}}_{\rm A}(n)$	$\hat{\mathfrak{M}}_{\rm B}(n)$	$\hat{\mathfrak{M}}_{\rm C}(n)$
0	48.7 ± 31.9	0.7 ± 0.5	12.6 ± 5.1	11.5 ± 4.9
2	49.1 ± 32.9	4.0 ± 3.3	12.6 ± 6.4	11.5 ± 6.3
5	47.1 ± 33.2	10.4 ± 8.8	14.5 ± 9.1	13.8 ± 8.9

one based on $\hat{\mathfrak{M}}_0(n)$. For $\mu_{P_{\rm LF}\%} \pm \sigma_{P_{\rm LF}\%}$, methods A, B, and C obtained similar results, which slightly increased when σ increased. For $\mu_{P_{\rm HF}\%} \pm \sigma_{P_{\rm HF}\%}$, approach A obtained notably lower values than approaches B and C.

Fig. 4 displays the averaged relative error trend $e_{\theta\%}(n)$ corresponding to $\hat{\mathfrak{M}}_0(n), \hat{\mathfrak{M}}_{\rm A}(n), \hat{\mathfrak{M}}_{\rm B}(n)$, and $\hat{\mathfrak{M}}_{\rm C}(n)$ for $\sigma = 2$ ms. Note that the average relative error trends $e_{\mathfrak{M}\%}(n), e_{P_{\rm LF}\%}(n)$, and $e_{P_{\rm HF}\%}(n)$, corresponding to the IPFM model with constant threshold [related to $\hat{\mathfrak{M}}_0(n)$], are dependent on the value of $T(t)$, being minimum when $T(t)$ equals its mean value and maximum for the lowest and highest values of $T(t)$. However, the average error trends corresponding to the TVIPFM model [related to $\hat{\mathfrak{M}}_{\rm A}(n), \hat{\mathfrak{M}}_{\rm B}(n)$, and $\hat{\mathfrak{M}}_{\rm C}(n)$] do not depend on the value of $T(t)$, although a peak is observed in the vicinity of stress peak, where there is an abrupt nonphysiological change in $T(t)$, which can not be followed by $\hat{d}_{\rm HRM}(n)$.

B. Stress Testing Database

From the $\hat{t}_k$ series estimated from the stress testing recordings described in Section II-C2, the modulating signal is estimated using $\hat{\mathfrak{M}}_0(n)$ and $\hat{\mathfrak{M}}_{\rm A}(n)$. Estimates $\hat{\mathfrak{M}}_0(n)$ and $\hat{\mathfrak{M}}_{\rm A}(n)$ are then filtered with a time-varying filter centered on the respiratory frequency [21] with a bandwidth of 0.14 Hz, and the envelopes of the filtered signals denoted as $\hat{b}_{\mathfrak{M}_{0,\rm HF}}(n)$ and $\hat{b}_{\mathfrak{M}_{\rm A,HF}}(n)$, respectively. Estimates $\hat{\mathfrak{M}}_0(n), \hat{\mathfrak{M}}_{\rm A}(n), \hat{b}_{\mathfrak{M}_{0,\rm HF}}(n)$, $\hat{b}_{\mathfrak{M}_{\rm A,HF}}(n), \hat{b}_{\mathfrak{M}_{\rm A,HF}}(n) - \hat{b}_{\mathfrak{M}_{0,\rm HF}}(n)$, and $\hat{d}_{\rm HRM}(n)$ are displayed in Fig. 5 for one of the subjects (with less than 10 h training per week), who performed the stress test at a pedalling frequency of 75 r/min. It can be appreciated that differences between $\hat{b}_{\mathfrak{M}_{0,\rm HF}}(n)$ and $\hat{b}_{\mathfrak{M}_{\rm A,HF}}(n)$ depend on the time-varying mean heart rate $\hat{d}_{\rm HRM}(n)$ being larger when $\hat{d}_{\rm HRM}(n)$ departs from its mean value. This can lead to erroneous interpretation of the ANS response to exercise when estimating its evolution from the changes observed in the estimated modulating signal. By using $\hat{\mathfrak{M}}_0(n)$ in this example, the return of the vagal activity [measured from $\hat{b}_{\mathfrak{M}_{0,\rm HF}}(n)$] observed in the early stage of the recovery (from second 1200 to 1400) reaches similar values than those corresponding to the beginning of the exercise (before second 300). This conclusion is slightly different by using $\hat{b}_{\mathfrak{M}_{\rm A,HF}}(n)$, where the two levels are different. Indeed, the latter conclusion is more likely from a physiological point of view [32].

In order to quantify the differences in the estimation of the modulating signal using the IPFM model with constant or time-varying threshold, the mean and SD of the difference between $\hat{b}_{\mathfrak{M}_{\rm A,HF}}(n)$ and $\hat{b}_{\mathfrak{M}_{0,\rm HF}}(n)$ are computed for each subject of Section II-C2, and then averaged among the 23 subjects, yielding a result of 10.5% ± 27.5% with respect to $\hat{\mathfrak{M}}_{\rm A}(n)$. This difference is of 50.6% ± 3.8% during the initial 5-min resting period and of −7.7% ± 14.3% during the first 2 min of the recovery phase, confirming the observation made from the example of Fig. 5, i.e., $\hat{\mathfrak{M}}_0(n)$ tends to overestimate vagal activity during the recovery and to underestimate it during the initial rest.

Inspection of Fig. 5 reveals an abrupt increase in $\hat{d}_{\rm HRM}(n)$ just after the onset of exercise (second 300), which is visible in all subjects of the database and may be due to the central command or the exercise pressor reflex in response to exercise [33]. The plateau observed from second 300 to 450, visible in some but not all the subjects, corresponds to the lowest intensity exercise and it may be associated to a transient response of the ANS at the onset of exercise. Note that a similar plateau is also observed in $\hat{b}_{\mathfrak{M}_{\rm A,HF}}(n)$ at lower values than those during rest, which then decreases concomitant with the linear increase in $\hat{d}_{\rm HRM}(n)$, until second 1000, when it slightly increases. During the recovery, there is an abrupt increase in $\hat{b}_{\mathfrak{M}_{\rm A,HF}}(n)$, which gradually decreases as the heart rate decreases, reaching values close to those observed during exercise. There is evidence that

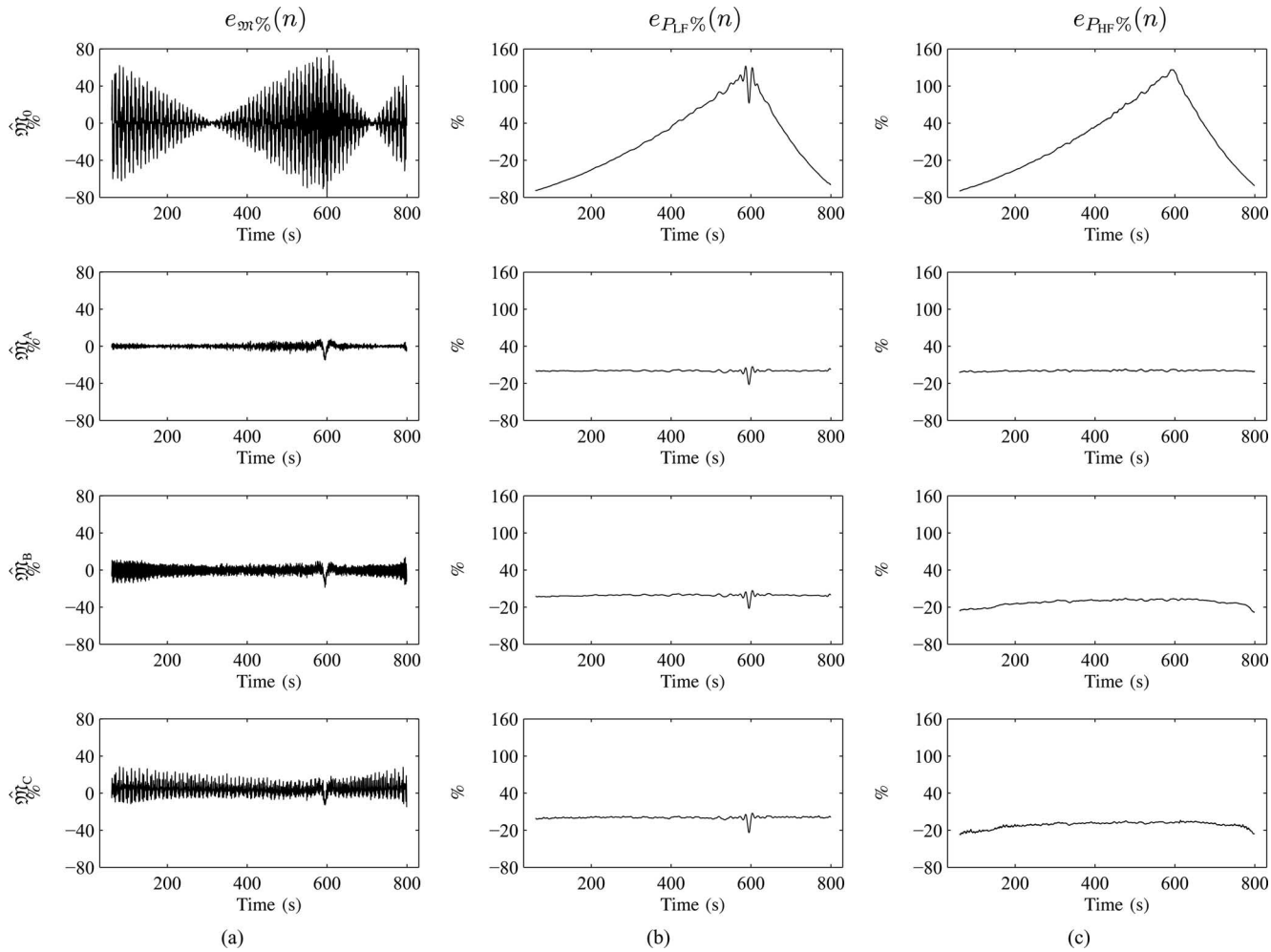

Fig. 4. Average relative error trend (a) $e_{\mathfrak{M}\%}(n)$, (b) $e_{P_{\mathrm{LF}}\%}(n)$, and (c) $e_{P_{\mathrm{HF}}\%}(n)$, corresponding, from top to bottom, to $\hat{\mathfrak{M}}_{0}(n)$, $\hat{\mathfrak{M}}_{\mathrm{A}}(n)$, $\hat{\mathfrak{M}}_{\mathrm{B}}(n)$, and $\hat{\mathfrak{M}}_{\mathrm{C}}(n)$, for $\sigma = 2$ ms.

the HF power, as well as other HRV indices, remains reduced with respect to resting values after 5, 10, 15, 30 min, or even an hour of the cessation of exercise [32], depending on exercise intensity and modality [34].

IV. Discussion

A. Methodological Aspects

In this paper, the TVIPFM model is applied to the analysis of HRV during exercise stress testing.

The classical IPFM model has been previously used in HRV analysis to estimate the ANS modulation on the heart from the beat occurrence time series, even in the presence of isolated ectopic beats, when the mean heart period can be considered constant [18], [19]. However, in situations, in which the mean heart period is time varying, such as during exercise stress testing, the estimation of the modulating signal in (1) needs to be modified, as proposed in (10), to account for the mean heart period modulation.

Three approaches have been considered to analyze the TVIPFM model, which allow the estimation of the modulating signal using the methods derived for the IPFM model with constant threshold plus a correction, which takes into account the time-varying threshold. The three approaches are based on the hypothesis that, in the time-varying threshold case, the instantaneous heart rate, derived as in the classical IPFM model, can be written as $d_{\mathrm{HR}}(t) = (1 + \mathfrak{m}(t))/T(t)$. A time-varying mean heart rate, which is the inverse of the time-varying mean heart period, is estimated by low-pass filtering $d_{\mathrm{HR}}(t)$. Approach A estimates the modulating signal multiplying the HRV signal with the time-varying mean heart period; approach B, dividing the variability of the heart period signal by the heart period signal itself; and approach C, dividing the variability of the heart period signal by the time-varying mean heart period.

Results from the simulation study show that the three approaches estimate the modulating signal as well as clinical HRV parameters with lower error than the classical IPFM model with constant threshold, being the differences larger for lower levels of noise. Approaches A, B, and C estimate the modulating signal with similar errors, being approach A the one achieving the lowest error in the absence of noise ($1.1\% \pm 1.3\%$). In the presence of high levels of noise ($\sigma = 5$ ms), approaches B and C obtained lower estimation errors than approach A, which can be due to the low pass-filtering effect associated to the heart period

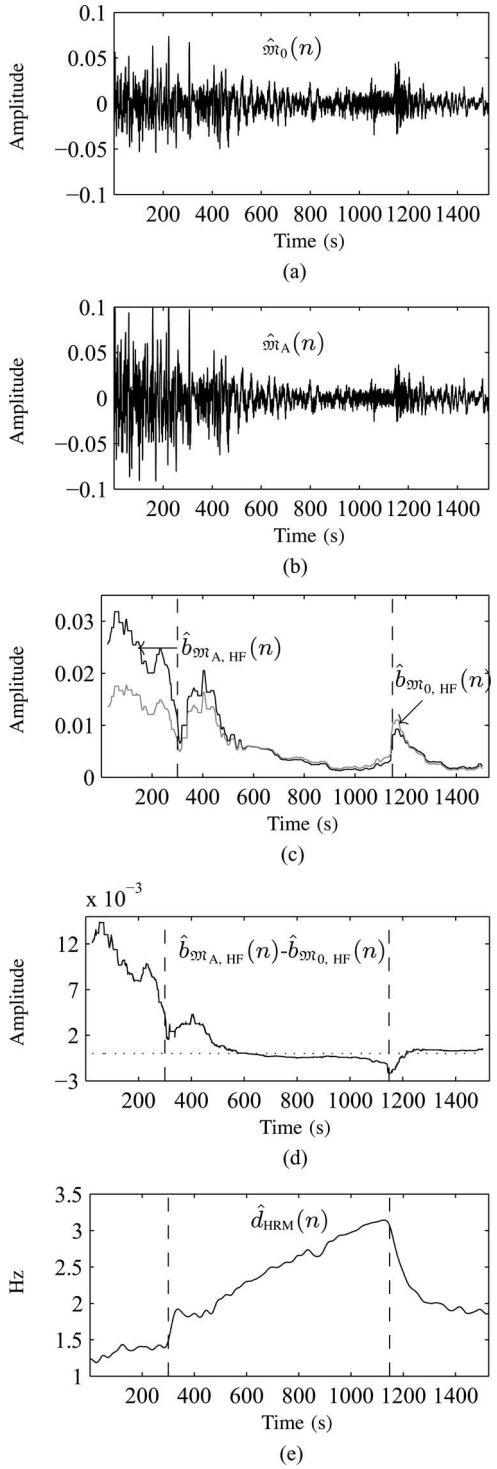

Fig. 5. Estimates for one of the subjects of Section II-C2: (a) $\hat{\mathfrak{M}}_0(n)$; (b) $\hat{\mathfrak{M}}_{\mathrm{A}}(n)$; (c) $\hat{b}_{\mathfrak{M}_{0,\mathrm{HF}}}(n)$ (grey) and $\hat{b}_{\mathfrak{M}_{\mathrm{A,HF}}}(n)$ (black); (d) $\hat{b}_{\mathfrak{M}_{\mathrm{A,HF}}}(n)$-$\hat{b}_{\mathfrak{M}_{0,\mathrm{HF}}}(n)$; and (e) $\hat{d}_{\mathrm{HRM}}(n)$.

signal on which approaches B and C are based [18]. It is worth noting that, while the power of the LF component is estimated with similar errors by the three approaches for all levels of noise, the power of the HF component is estimated with notably lower error by approach A (0.7% ± 0.5%) than by approaches B (12.6% ± 5.1%) and C (11.5% ± 4.9%). This, again, can be explained by the low-pass-filtering effect when estimating HRV from the heart period signal [18], and is not related to the influence of sympathetic and parasympathetic stimulations on the sinus node. An alternative approach for the estimation of approaches B and C, which is not based on $d_{\mathrm{HR}}(t)$, but only on the heart period $d_{\mathrm{HP}}(t)$ signal is considered in Appendix A, yielding similar results (not shown).

In this paper, a time-varying HF band centered on the respiratory frequency [31] has been considered both in the simulation study and in the stress testing database. When a simultaneously recorded respiration signal is not available, respiratory frequency can be derived from the ECG signal using, e.g., the method described in [26], which has been shown to provide reliable respiratory frequency estimates during stress testing.

The TVIPFM has been also applied to the analysis of HRV in [24], where the modulating signal as well as the time-varying threshold are decomposed into a series of orthogonal basis functions. Despite its computational complexity, one of the advantages of the method in [24] is that it does not require the time-varying threshold to be of lower frequency than the modulating signal. However, the application of the method in [24] to the analysis of HRV during exercise stress testing requires further considerations since the frequency band covered by the basis functions depends on the mean heart rate, which is time-varying during exercise stress testing. If the most restrictive frequency band, given by the lowest mean heart rate, is chosen for the basis functions, it may not be large enough to include the LF as well as the HF components, centered on respiratory frequency, or even other components such as the pedaling component, when the exercise intensity is high. This could be overcome by performing the analysis in short-time intervals, whose length is inversely proportional to the frequency resolution of the basis functions.

A note of caution should be considered when using different representations of HRV, since the effect of a time-varying mean heart rate may be different. For example, if the power of the LF and HF components are obtained from the heart rate signal, an increase in mean heart rate leads to an overestimation of the modulating signal (see Figs. 3, 4, and 5), while if the heart period signal is used, it leads to an underestimation of the modulating signal [20], [21], [25] (see Appendix B for an analytical example). The later case is, in fact, an interpretation of approaches B and C.

B. Physiological Aspects

An important result derived from the simulation study is that the estimation error of the modulating signal (and of the clinical HRV parameters) obtained by the classical IPFM model is dependent on the value of the time-varying threshold, while it does not depend on it when the TVIPFM model is considered. This is of particular importance when the ANS evolution is estimated from the changes observed in the estimated modulating signal (or in the clinical HRV parameters) and may lead to erroneous interpretation of the ANS response to exercise. One example is the mechanical stretching modulation of the sinus node due to respiration, which may be overestimated if the time-varying threshold is not considered. Another example is the return of

vagal activity during recovery, which is relevant in stress testing studies [35], [36] and may be overestimated by the IPFM model with constant threshold.

The suitability of the TVIPFM model to the analysis of HRV during exercise stress testing may be justified by the observation that the mean heart period is not constant during the exercise, but increases with work load to satisfy the increasing metabolic demand. But the TVIPFM model may be useful for the analysis of HRV in a wider context. It is worth mentioning that threshold modulation was first introduced in the classical IPFM model in order to study the possibility of transmitting two informations, with potentially different sources, along the same channel [22]. The TVIPFM has been applied to HRV analysis in [24] to discriminate between the ANS modulation of the SA node and the stretch-induced effect, since there is evidence that the variations in sinus rhythm caused by autonomic modulation and stretch-induced variations are mediated through different mechanisms: the rate of depolarization for the former and the threshold level for the later. Moreover, the autonomic modulation itself has been shown to affect the sinus rhythm through different mechanisms. For example, the stimulation of the sympathetic nerves releases the hormone norepinephrine, which is believed to increase the permeability of the fiber membrane to sodium and calcium ions, which in turn, causes a more positive resting potential, and also causes increased rate of upward drift of the membrane potential during diastolic depolarization [37]. Parasympathetic stimulation releases acetylcholine, which may cause a decrease in the slope of diastolic depolarization, an increase (in absolute value) in maximum diastolic potential, and an increase in the threshold potential [38], [39]. In the TVIPFM model, the changes in the slope of the diastolic depolarization membrane potential can be modeled by the modulating signal $\mathfrak{m}(t)$, while changes in both threshold potential and maximum diastolic potential may be modeled by the time-varying threshold $T(t)$.

One of the limitations of the TVIPFM model concerning the physiological interpretation of HRV is that it cannot distinguish from different sources of sympathetic or parasympathetic stimulations, which share the same frequency band.

V. Conclusion

In this paper, a new technique for the analysis of HRV during exercise stress testing has been introduced based on the TVIPFM model. On a simulation study, this technique allows the estimation of the ANS modulation on the heart from the beat occurrence time series with lower bias and SD than the classical IPFM model with constant threshold. Estimation errors achieved by this technique are independent from the time-varying mean heart rate, as opposed to the ones obtained by the classical IPFM model. On an exercise stress testing database, the ANS modulation estimated by the proposed technique is closer to physiology than that obtained from the classical IPFM model with constant threshold. In situations where HRV measurements at different mean heart periods are compared, the proposed correction of HRV measurements with the time-varying mean heart rate should be considered.

Appendix A

An alternative approach for the estimation of $\hat{T}(t_{k_c})$, which may be used in (19) and (20), is the following. Note that thanks to (19) and assuming that $\mathfrak{m}(t_{k_c})$ is small compared to 1, the heart period signal, estimated by the interval function, can be written as follows:

$$\begin{aligned}\hat{d}_{\mathrm{HP}}(t_k) = d_{\mathrm{IF}}(t_k) = t_k - t_{k-1} &= \frac{T(t_{k_c})}{1+\mathfrak{m}(t_{k_c})} \\ &\approx T(t_{k_c})\left[1-\mathfrak{m}(t_{k_c})\right] \approx T(t_{k_c}) - T(t_{k_c})\,\mathfrak{m}(t_{k_c})\end{aligned} \tag{29}$$

which can be considered to be approximately composed of a low-pass component $T(t_{k_c})$ and a high-pass component $T(t_{k_c})\,\mathfrak{m}(t_{k_c})$. Assuming that $T(t)$ is of lower frequency and $\mathfrak{m}(t)$ of higher frequency, the separation of lower and higher frequency components is straightforward. Therefore, $\hat{T}(t_{k_c})$ is easily computed low-pass filtering $\hat{d}_{\mathrm{HP}}(t_k)$, and, consequently, $\hat{\mathfrak{m}}(t_{k_c})$ by using (19) or (20).

Appendix B

Using as modulating signal $\mathfrak{m}(t) = A\cos(2\pi f_1 t)$ into the IPFM model (1) for successive beats leads to

$$t_k - t_{k-1} + \frac{A}{2\pi f_1}\left(\sin(2\pi f_1 t_k) - \sin(2\pi f_1 t_{k-1})\right) = T. \tag{30}$$

If $f_1(t_k - t_{k-1}) \approx f_1 T \ll 1$, the heart period signal, estimated by the interval function, can be written as follows [25]:

$$\hat{d}_{\mathrm{HP}}(t_k) \approx T - AT\cos(\pi f_1(2t_k - T)) \tag{31}$$

which represents an estimate of $\mathfrak{m}(t)$ with a scaling factor proportional to the mean heart period T. If $A \ll 1$, the heart rate signal, estimated by the inverse interval function $\hat{d}_{\mathrm{HR}}(t_k) = d_{\mathrm{IIF}}(t_k) = 1/(t_k - t_{k-1})$, can be written as follows:

$$\hat{d}_{\mathrm{HR}}(t_k) \approx \frac{1}{T} + \frac{A}{T}\cos(\pi f_1(2t_k - T)) \tag{32}$$

which, in contrast with the heart period signal, represents an estimate of $\mathfrak{m}(t)$ with a scaling factor inversely proportional to T.

Acknowledgment

The authors would like to thank Dr. G. Blain and Dr. S. Bermon for providing the exercise stress data.

References

[1] E. Bayly, "Spectral analysis of pulse frequency modulation in the nervous system," *IEEE Trans. Biomed. Eng.*, vol. BME-15, no. 4, pp. 257–265, Oct. 1968.

[2] B. Hyndman and R. Mohn, "A model of the cardiac pacemaker and its use in decoding the information content of cardiac intervals," *Automedica*, vol. 1, pp. 239–252, 1975.

[3] A. Sanderson, "Input-output analysis of an IPFM neural model: Effects of spike regularity and record length," *IEEE Trans. Biomed. Eng.*, vol. BME-27, no. 3, pp. 120–131, Mar. 1980.

[4] O. Rompelman, A. Coenen, and R. Kitney, "Measurement of heart rate variability—Part 1: Comparative study of heart rate variability analysis methods," *Med. Biol. Eng. Comput.*, vol. 15, pp. 239–252, 1977.

[5] O. Rompelman, J. Snijders, and C. van Spronsen, "The measurement of heart rate variability spectra with the help of a personal computer," *IEEE Trans. Biomed. Eng.*, vol. BME-29, no. 7, pp. 503–510, Jul. 1982.
[6] R. DeBoer, J. Karemaker, and J. Strackee, "Comparing spectra of a series of point events particularly for heart rate variability data," *IEEE Trans. Biomed. Eng.*, vol. BME-31, no. 4, pp. 384–387, Apr. 1984.
[7] R. DeBoer, J. Karemaker, and J. Strackee, "Spectrum of a series of point event, generated by the integral pulse frequency modulation model," *Med. Biol. Eng. Comput.*, vol. 23, pp. 138–142, 1985.
[8] R. D. Berger, S. Akeselrod, D. Gordon, and R. J. Cohen, "An efficient algorithm for spectral analysis of heart rate variability," *IEEE Trans. Biomed. Eng.*, vol. BME-33, no. 9, pp. 900–904, Sep. 1986.
[9] P. Castiglioni, "Evaluation of heart rhythm variability by heart or heart period: Differences, pitfalls and help from logarithms," *Med. Biol. Eng. Comput.*, vol. 33, pp. 323–330, 1995.
[10] M. Brennan, M. Palaniswami, and P. Kamen, "Distortion properties of the interval spectrum of IPFM generated heartbeats for heart rate variability analysis," *IEEE Trans. Biomed. Eng.*, vol. 48, no. 11, pp. 1251–1264, Nov. 2001.
[11] M. Brennan, M. Palaniswami, and P. Kamen, "Poincaré plot interpretation using a physiological model of HRV based on a network of oscillators," *Amer. J. Physiol. Heart Circ. Physiol.*, vol. 283, pp. H1873–H1886, 2002.
[12] R. Bailón, L. Mainardi, M. Orini, L. Sörnmo, and P. Laguna, "Analysis of heart rate variability during exercise stress testing using respiratory information," *Biomed. Signal Process Control*, vol. 5, pp. 299–310, 2010.
[13] L. Mainardi, A. Bianchi, and S. Cerutti, "Time-frequency and time-varying analysis for assessing the dynamic responses of cardiovascular control," *Crit. Rev. Biomed. Eng.*, vol. 30, no. 1–2, pp. 181–223, 2002.
[14] M. Orini, R. Bailón, R. Enk, S. Koelsch, L. Mainardi, and P. Laguna, "A method for continuously assessing the autonomic response to music-induced emotions through HRV analysis," *Med. Biol. Eng. Comput.*, vol. 48, pp. 423–433, May 2010.
[15] The Task Force of ESC NASPE, "Heart rate variability. Standards of measurement, physiological interpretation, and clinical use," *Eur. Heart J.*, vol. 17, pp. 354–381, 1996.
[16] A. Bianchi, L. Mainardi, E. Petrucci, M. Signorini, M. Mainardi, and S. Cerutti, "Time-variant power spectrum analysis for the detection of transient episodes in HRV signal," *IEEE Trans. Biomed. Eng.*, vol. 40, no. 2, pp. 136–144, Feb. 1993.
[17] F. Lombardi, A. Malliani, M. Pagani, and S. Cerutti, "Heart rate variability and its sympatho-vagal modulation," *Cardiovasc. Res.*, vol. 32, pp. 208–216, 1996.
[18] J. Mateo and P. Laguna, "Improved heart rate variability time-domain signal construction from the beat occurrence times according to the IPFM model," *IEEE Trans. Biomed. Eng.*, vol. 47, no. 8, pp. 985–996, Aug. 2000.
[19] J. Mateo and P. Laguna, "Analysis of heart rate variability in the presence of ectopic beats using the heart timing signal," *IEEE Trans. Biomed. Eng.*, vol. 50, no. 3, pp. 334–343, Mar. 2003.
[20] H. Chiu, T. Wang, L. Huang, H. Tso, and T. Kao, "The influence of mean heart rate on measures of heart rate variability as markers of autonomic function: A model study," *Med. Eng. Phys.*, vol. 25, pp. 475–481, 2003.
[21] O. Meste, B. Khaddoumi, G. Blain, and S. Bermon, "Time-varying analysis methods and models for the respiratory and cardiac system coupling in graded exercise," *IEEE Trans. Biomed. Eng.*, vol. 52, no. 11, pp. 1921–1930, Nov. 2005.
[22] J. Galván, "Introducing threshold modulation in Bayly's integral pulse frequency modulation in the neuron," *Proc. IEEE*, vol. 63, no. 11, pp. 733–734, Apr. 1975.
[23] J. Kong, Y.-T. Zhang, and W. X. Lue, "Dynamical behaviours of integral pulse frequency modulation (IPFM) model with a periodically-varied threshold," in *Proc. 1st Joint BMES/EMBS Conf.*, Piscataway, NJ: IEEE Press, 1999, vol. 2, p. 1000.
[24] S. Seydnejad and R. Kitney, "Time-varying threshold integral pulse frequency modulation," *IEEE Trans. Biomed. Eng.*, vol. 48, no. 9, pp. 949–962, Sep. 2001.
[25] G. Laouini, A. Cabasson, G. Blain, P. Bonizzi, O. Meste, and S. Bermon, "Evidence of the influence of respiration on the heart rate variability after human heart transplantation: Role of observation model," *Comput. Cardiol.*, Sep. 13–16, 2009, pp. 409–412.
[26] R. Bailón, L. Sörnmo, and P. Laguna, "A robust method for ECG-based estimation of the respiratory frequency during stress testing," *IEEE Trans. Biomed. Eng.*, vol. 53, no. 7, pp. 1273–1285, Jul. 2006.
[27] Y. Arai, J. Saul, P. Albrecht, L. Hartley, L. Lilly, R. Cohen, and W. Colucci, "Modulation of cardiac autonomic activity during and immediately after exercise," *Amer. J. Physiol. Heart Circ. Physiol.*, vol. 256, pp. H132–H141, 1989.
[28] K. Shin, H. Minamitani, S. Onishi, H. Yamazaki, and M. Lee, "The power spectral analysis of heart rate variability in athletes during dynamic exercise—Part I," *Clin. Cardiol.*, vol. 18, pp. 583–586, 1995.
[29] K. Shin, H. Minamitani, S. Onishi, H. Yamazaki, and M. Lee, "The power spectral analysis of heart rate variability in athletes during dynamic exercise—Part II," *Clin. Cardiol.*, vol. 18, pp. 664–668, 1995.
[30] G. Blain, O. Meste, A. Blain, and S. Bermon, "Time–frequency analysis of heart rate variability reveals cardiolocomotor coupling during dynamic cycling exercise in humans," *Amer. J. Physiol. Heart Circ. Physiol.*, vol. 296, pp. 1651–1659, 2009.
[31] R. Bailón, P. Laguna, L. Mainardi, and L. Sörnmo, "Analysis of heart rate variability using time-varying frequency bands based on respiratory frequency," in *Proc. 29th Int. Conf. IEEE Eng. Med. Biol. Soc.*, IEEE-EMBS Society, Lyon, 2007, pp. 6674–6677.
[32] O. Barak, D. Jakovljevic, J. P. Gacesa, Z. Ovcin, D. Brodie, and N. Grujic, "Heart rate variability before and after cycle exercise in relation to different body positions," *J. Sports Sci. Med.*, vol. 9, pp. 176–182, 2010.
[33] F. Iellamo, "Neural control of the cardiovascular system during exercise," *Ital. Heart J.*, vol. 2, no. 3, pp. 200–212, 2001.
[34] V. Gladwell, G. Sandercock, and S. Birch, "Cardiac vagal activity following three intensities of exercise in humans," *Clin. Physiol. Funct. Imaging*, vol. 30, pp. 17–22, 2010.
[35] F. Dewey, J. Freeman, G. Engel, R. Oviedo, N. Abrol, N. Ahmed, J. Myers, and V. Froelicher, "Novel predictor of prognosis from exercise stress testing: Heart rate variability response to the exercise treadmill test," *Amer. Heart J.*, vol. 153, pp. 281–288, 2007.
[36] J. Leino, M. Virtanen, M. Kähönen, K. Nikus, T. Lehtimäki, T. Kööbi, R. Lehtinen, V. Turjanmaa, J. Viik, and T. Nieminen, "Exercise-test-related heart rate variability and mortality: The Finnish cardiovascular study," *Int. J. Cardiol.*, vol. 144, no. 1, pp. 154–155, Sep. 2010. DOI: 10.1016/j.ijcard.2008.12.123
[37] A. Guyton, *Textbook of Medical Physiology*. Philadelphia, PA: Saunders, 2005.
[38] B. Hoffman, "Autonomic control of cardiac rhythm," *Bull. N.Y. Acad. Med.*, vol. 43, no. 12, pp. 1087–1096, 1967.
[39] A. Bucchi, M. Baruscotti, R. Robinson, and D. DiFrancesco, "Modulation of rate by autonomic agonists in SAN cells involves changes in diastolic depolarization and the pacemaker current," *J. Mol. Cell. Cardiol.*, vol. 43, pp. 39–48, 2007.

Raquel Bailón was born in Zaragoza, Spain, in 1978. She received the M.Sc. degree in telecommunication engineering and the Ph.D. degree in biomedical engineering from the University of Zaragoza (UZ), Zaragoza, Spain, in 2001 and 2006, respectively.

In 2003, she was an Assistant Professor in the Department of Electronic Engineering and Communications, UZ, where she is an Associate Professor since 2010. She is also a Researcher with the Aragón Institute for Engineering Research, UZ, and also with the Centro de Investigación Biomédica en Red en Bioingeniería, Biomateriales y Nanomedicina, 50018 Zaragoza, Spain. Her current research interests include the biomedical signal processing field, specially in the analysis of the dynamics and interactions of cardiovascular signals.

Ghailen Laouini received the M.Sc. degree in applied mathematics from the University of Pierre et Marie Curie, Paris, France, in 2008. He is currently working toward the Ph.D. Degree in automatic and signal processing at the BIOMED project at the Laboratory of Informatics, Signals and Systems (I3S), University of Nice Sophia Antipolis, Nice, France.

César Grao was born in Teruel, Spain, in 1985. He received the M.Sc. degree in telecommunications engineering from the University of Zaragoza (UZ), Zaragoza, Spain, in 2009. He is a student at the University of Zaragoza.

Michele Orini received the M.S. degree in biomedical engineering from the Politecnico di Milano, Milano, Italy, and the engineer degree from the École Céntrale Paris, France. He is currently working toward the Ph.D. degree in biomedical engineering at the University of Zaragoza, Zaragoza, Spain, and the Politecnico di Milano.

His research interest includes nonstationary biomedical signal processing and focuses on the dynamic interactions between cardiovascular signals.

Pablo Laguna (SM'06) was born in Jaca (Huesca), Spain, in 1962. He received the M.S. degree in physics and the Ph.D. degree in physical science from the Science Faculty, University of Zaragoza, Zaragoza, Spain, in 1985 and 1990, respectively. The Ph.D. thesis was developed at the Biomedical Engineering Division, Institute of Cybernetics [Polytechnic University of Catalonia-Spanish Council of Scientific Research (UPC-CSIC)].

He is currently a Full Professor of Signal Processing and Communications in the Department of Electrical Engineering, Engineering School, and a Researcher at the Aragón Institute for Engineering Research (I3A), both at University of Zaragoza, where he was an Associated Professor from 1992 to 2005. He was an Assistant Professor of Automatic Control in the Department of Control Engineering, Polytechnic University of Catalonia (UPC), Barcelona, Spain, and a Researcher at the Biomedical Engineering Division, Institute of Cybernetics (UPC-CSIC). His professional research interest includes signal processing, in particular applied to biomedical applications. He is, together with L. Sörnmo, the author of *Bioelectrical Signal Processing in Cardiac and Neurological Applications* (Elsevier, 2005).

Dr. Laguna is also a member of the El Centro de Investigación Biomédica en Red en Bioingeniería, Biomateriales y Nanomedicina (CIBER-BBN) Research Center, Instituto de Salud Carlos III, Spanish Ministry of Science and Innovation.

Olivier Meste (M'97) received the M.Sc. degree in automatic and signal processing and the Ph.D. degree in scientific engineering from the University of Nice-Sophia Antipolis, Nice, France, in 1989 and 1992, respectively.

He is currently a Full Professor at the University of Nice-Sophia Antipolis and a Researcher at the Laboratory of Informatics, Signals and Systems (I3S), Nice. His research interests include digital processing, time-frequency representations, and modeling of biological signals and systems, including ECG, EMG, and EEG.

Dr. Meste is a member of the Bio Imaging and Signal Processing technical committee of the IEEE Signal Processing Society.